PCCP

PAPER

View Article Online
View Journal | View Issue

Cite this: *Phys. Chem. Chem. Phys.*, 2015, **17**, 23748

^{14}N overtone transition in double rotation solid-state NMR†

Ibraheem M. Haies,[ab] James A. Jarvis,[c] Lynda J. Brown,[a] Ilya Kuprov,[a] Philip T. F. Williamson[c] and Marina Carravetta*[a]

Received 5th June 2015,
Accepted 4th August 2015

DOI: 10.1039/c5cp03266k

www.rsc.org/pccp

Solid-state NMR transitions involving outer energy levels of the spin-1 ^{14}N nucleus are immune, to first order in perturbation theory, to the broadening caused by the nuclear quadrupole interaction. The corresponding overtone spectra, when acquired in conjunction with magic-angle sample spinning, result in lines, which are just a few kHz wide, permitting the direct detection of nitrogen compounds without the need for labeling. Despite the success of this technique, "overtone" resonances are still broadened due to indirect, second order effects arising from the large quadrupolar interaction. Here we demonstrate that another order of magnitude in spectral resolution may be gained by using double rotation. This brings the width of the ^{14}N solid-state NMR lines much closer to the region commonly associated with high-resolution solid-state NMR spectroscopy of ^{15}N and demonstrates the improvements in resolution that may be possible through the development of pulsed methodologies to suppress these second order effects.

Introduction

Nitrogen is one of the most abundant elements in nature, but most nitrogen NMR studies have so far been restricted to the ^{15}N isotope (natural abundance $\sim$0.4%) to avoid problems associated with the large ^{14}N quadrupolar interaction, often in the MHz range.[1–4] Significant attention has been given to the possibility of developing high-resolution versions of ^{14}N solid state NMR to ease the acquisition of data without isotopic labelling, as well as to harvest additional information on the nitrogen site and its environment as provided by the quadrupolar interaction. This has led to the development of a number of promising techniques including ultra-wideband acquisition,[2,3,5] indirect detection[4,6–14] and excitation of ^{14}N overtone transitions.[15–24] Overtone NMR spectroscopy is advantageous because the width of the ^{14}N overtone powder pattern is unaffected, to first order in perturbation theory, by the quadrupolar interaction.[25] The experimental feasibility of directly detecting the ^{14}N overtone transition by NMR was first demonstrated in the 1980's by Tycko and Opella on static samples.[21–23,25] More recently, ^{14}N overtone spectra acquired under magic-angle spinning (MAS) have been reported, demonstrating the existence of only five ^{14}N spinning sidebands.[17,24] However, even under MAS, the overtone powder line is still in the kHz range, due to the presence of quadrupolar interaction terms of the spherical rank higher than 2 in the effective Hamiltonian. Any further improvements in resolution will necessitate the removal of these terms. Several methods exist for the elimination of high-rank quadrupole interaction terms. For half-integer quadrupolar nuclei, MQMAS[26–28] and STMAS[29] methods remove them by modifying the spin part of the effective Hamiltonian. For the spatial part, double rotation (DOR)[30–32] and dynamic angle spinning (DAS)[31,33] achieve the same objective by mechanical averaging.

One of the main challenges for the routine application of ^{14}N solid state NMR is resolution. In this communication we address this issue and demonstrate experimentally that, when applied to ^{14}N overtone NMR, DOR can bring about a significant further reduction in line width and take the NMR lines into the sub-kHz domain more commonly associated with NMR of spin-1/2 nuclei. Information on the size of the quadrupolar interaction is still present in the DOR spectra as the peak position is determined by a combination of the chemical shift and the second order isotropic quadrupolar shift. A further challenge to tackle with methods for sensitivity enhancement is already being developed, including polarization transfer,[24] DNP,[20] optimal control theory[34] and other instrumental improvements.

We also report progress with another long-standing issue associated with both DOR and overtone spectroscopy – the mathematical complexity of its numerical treatment. This paper uses the Fokker–Planck formalism[35,36] (recently implemented in

[a] *School of Chemistry, University of Southampton, SO17 1BJ, Southampton, UK. E-mail: m.carravetta@soton.ac.uk*
[b] *Department of Chemistry, College of Science, University of Mosul, Mosul, Iraq*
[c] *Centre for Biological Sciences, University of Southampton, SO17 1BJ, Southampton, UK*

† Electronic supplementary information (ESI) available. See DOI: 10.1039/c5cp03266k

Spinach[37]). Its most attractive feature is that the DOR evolution operator is time-independent and the rotor coordinates, once discretized, are in a direct product relationship with the spin degrees of freedom.

Materials and methods

Solid state NMR

All the NMR measurements were performed on a Bruker AVANCE III 850 MHz spectrometer. All spectra were referenced indirectly to 0 ppm (liquid ammonia) using the ^{14}N signal of ammonium chloride at 39.3 ppm.[38] The overtone reference frequency was taken to be twice the ^{14}N reference frequency.

The DOR measurements used a wide-bore double resonance DOR probe, with diameters of 9.3 mm for the outer rotor (at magic angle) and 3.4 mm for the inner rotor (at 30.56°), respectively. Both rotors rotate in a clockwise direction. The power level was calibrated to give an overtone nutation frequency of $\omega_{\mathrm{nut}}^{\mathrm{OT}}/2\pi$ = 21 kHz for the ^{14}N overtone using the ^{17}O signal from the H_2O sample at 115.262 MHz and no ^{1}H decoupling was used under DOR.

MAS measurements were performed using a 3.2-mm-wide-bore triple resonance probe and a 3.2 mm zirconium oxide rotor, which rotates in the anticlockwise direction. For MAS, SPINAL64 decoupling at $\omega_{\mathrm{nut}}^{\mathrm{H}}/2\pi$ = 89 kHz was used throughout, while the overtone nutation frequency was set to $\omega_{\mathrm{nut}}^{\mathrm{OT}}/2\pi$ = 70 kHz and calibrated on water as above.

NMR samples

DOR experiments were performed on 27 mg of glycine-*N*,*N*,*O*-d_3 (Aldrich) and 24 mg of *N*-(acetyl-d_3)valine-d_{10} (NAV, prepared in house). The synthesis and characterization of fully deuterated NAV are described below. Deuterated samples were chosen for the DOR experiments due to the very limited ^{1}H decoupling performance of this probe. For the MAS measurements, 35 mg of naturally abundant glycine and 31 mg of naturally abundant NAV (both obtained from Sigma-Aldrich and used without further purification) were used. During MAS acquisition, SPINAL-64 decoupling was used with a nutation frequency of 89 kHz. All recycle delays were set to 0.5 s.

Synthesis of *N*-(acetyl-d_3)valine-d_{10}

Solvents and reagents were used as received from standard chemical suppliers unless otherwise stated. Fourier-transform infrared (FT-IR) spectra are reported in wavenumbers (cm^{-1}) and were collected on a Nicolet 380 spectrometer fitted with a diamond platform. ^{2}H and ^{13}C NMR spectra were recorded in CH_3OH/CD_3OD solutions (76.8 MHz and 100 MHz, respectively). Chemical shifts are reported in ppm relative to TMS and coupling constants (J) are reported in Hz with rounding to the nearest 0.1 Hz. Melting points are uncorrected. Electrospray mass spectra were obtained using a Micromass platform mass analyser with an electrospray ion source.

A clear solution was prepared by sonication of L-valine-d_8 (250 mg, 2 mmol) in D_2O (5 mL). Acetic anhydride-d_6 (433 mg, 4 mmol, 380 μL) was added at 0 min, 2 min and 4 min (127 μL at each interval). The reaction (Scheme 1) was sonicated for a further 5 min and then the solvent was removed *in vacuo*. The white residue was dissolved in methanol (20 mL) and the solution was filtered to remove traces of unreacted starting material. The filtrate was evaporated *in vacuo* and the residue was recrystallised twice from D_2O (2 × 1 mL) to give *N*-(acetyl-d_3)valine-d_{10} as a white solid (280 mg, 1.63 mmol, 82%). Further details of the characterization of this material are provided in the ESI.†

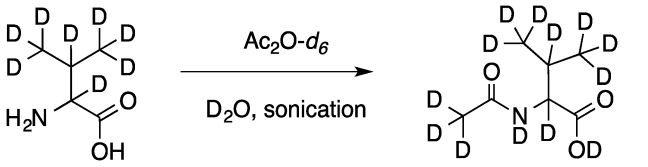

Scheme 1 Preparation of NAV.[39]

Theory

The recently proposed Fokker–Planck formalism for solid state NMR calculations[36,38] allows the simulation of double rotation overtone NMR experiments to be performed without undue formulaic complexity and in reasonable time. The primary observation is very similar to the one made in the stochastic Liouville equation theory[40,41] – spatial dynamics may be introduced into the equation of motion simply by adding the corresponding derivatives to the evolution generator. In the case of DOR NMR, we have

$$\frac{\partial}{\partial t}\hat{\rho}(\varphi_{\mathrm{O}},\varphi_{\mathrm{I}},t)=\left[-i\hat{\hat{H}}(\varphi_{\mathrm{O}},\varphi_{\mathrm{I}},t)+\omega_{\mathrm{O}}\frac{\partial}{\partial\varphi_{\mathrm{O}}}+\omega_{\mathrm{I}}\frac{\partial}{\partial\varphi_{\mathrm{I}}}\right]\hat{\rho}(\varphi_{\mathrm{O}},\varphi_{\mathrm{I}},t) \quad (1)$$

where $\varphi_{\mathrm{O,I}}$ are outer and inner rotor angles, $\omega_{\mathrm{O,I}}$ are outer and inner rotor angular frequencies, $\hat{\rho}(\varphi_{\mathrm{O}}, \varphi_{\mathrm{I}}, t)$ is the state vector and $\hat{\hat{H}}(\varphi_{\mathrm{O}},\varphi_{\mathrm{I}},t)$ is the spin Hamiltonian commutation superoperator:

$$\hat{\hat{H}}(\varphi_{\mathrm{O}},\varphi_{\mathrm{I}},t)=\hat{\hat{H}}_0(\varphi_{\mathrm{O}},\varphi_{\mathrm{I}})+\hat{\hat{H}}_1(t) \quad (2)$$

in which the dependence on the two spinner angles is parametric and the time-dependent part (radiofrequency pulses, *etc.*) is orientation-independent.

If the spatial basis is chosen to be complex exponentials of the rotor angles, this formalism would reduce[35] to nested Floquet theory.[42,43] eqn (1) does, however, also permit a more direct numerical approach – exact matrix representations exist for the derivative operators on any periodic grid.[44] At the matrix level, this leads to remarkably simple relations:

$$\begin{gathered}\frac{\partial}{\partial t}\boldsymbol{\rho}(t)=-i\mathbf{F}(t)\boldsymbol{\rho}(t),\quad \mathbf{F}(t)=\mathbf{H}_0+\mathbf{H}_1(t)+\mathbf{D}_{\mathrm{I}}+\mathbf{D}_{\mathrm{O}}\\ \mathbf{H}_1(t)=\hat{\hat{E}}_{N_{\mathrm{O}}}\otimes\hat{\hat{E}}_{N_{\mathrm{I}}}\otimes\hat{\hat{H}}_1(t),\quad \mathbf{D}_{\mathrm{I}}=i\omega_{\mathrm{I}}\hat{\hat{E}}_{N_{\mathrm{O}}}\otimes\hat{\hat{D}}_{N_{\mathrm{I}}}\otimes\hat{\hat{E}}_{N_{\mathrm{S}}},\\ \mathbf{D}_{\mathrm{O}}=i\omega_{\mathrm{O}}\hat{\hat{D}}_{N_{\mathrm{O}}}\otimes\hat{\hat{E}}_{N_{\mathrm{I}}}\otimes\hat{\hat{E}}_{N_{\mathrm{S}}}\end{gathered} \quad (3)$$

where N_{O} is the number of grid points for the outer rotor, N_{I} is the number of grid points for the inner rotor, N_{S} is the

dimension of the spin state space, $\hat{\hat{E}}$ are identity superoperators of indicated dimensions, $\hat{\hat{D}}$ are Fourier spectral differentiation matrices[44] of indicated dimensions, the vector $\boldsymbol{\rho}(t)$ is obtained by stacking the state vector $\hat{\rho}(\varphi_{\mathrm{O}}^{(n)}, \varphi_{\mathrm{I}}^{(k)}, t)$ vertically in the order of increasing index of the inner rotor grid points, followed by the increasing index of the outer rotor grid points, and the block-diagonal matrix $\mathbf{H}_0$ is obtained by concatenating individual grid point Hamiltonians $\hat{H}_0(\varphi_{\mathrm{O}}^{(n)}, \varphi_{\mathrm{I}}^{(k)})$ in the same order as the state vectors.

From the practical programming perspective, the entire procedure is implemented and extensively annotated in the double rotation module of *Spinach.*[37] At the cost of increasing the matrix dimensions, the presence of the double rotation no longer troubles the end user – DOR dynamics operators are now just another static term in the background Hamiltonian $\mathbf{F}_0$:

$$\mathbf{F}(t) = \mathbf{F}_0 + \mathbf{F}_1(t), \quad \mathbf{F}_0 = \mathbf{H}_0 + \mathbf{D}_{\mathrm{I}} + \mathbf{D}_{\mathrm{O}}, \quad \mathbf{F}_1(t) = \mathbf{H}_1(t) \qquad (4)$$

Another advantage of eqn (3) is that averages with respect to the phases of both rotors may be computed simply by taking the average of every block in $\boldsymbol{\rho}(t)$. This means that a powder simulation would only need a two-angle spherical averaging grid. In principle, even that is not strictly necessary,[37] but the mathematics in the grid-free case is less straightforward.

From this point onwards, the problem is identical to the simulation of a pulse-acquire experiment with a soft pulse, with the additional complication that the frequency of the pulse is *twice* the Larmor frequency of the spin – we are pulsing and detecting the overtone transition. The methods used to perform such simulations in reasonable time are described in our previous paper[24] and implemented in *Spinach.*[37] Because the number of spinning sidebands in overtone spectra is small and the resulting signals are narrow, five to seven grid points for the discretization of the phase of each rotor and a rank 5 Lebedev spherical averaging grid (parallel evaluation) were in practice found to be sufficient. When the calculation is parallelized with respect to the spherical averaging grid, the simulation shown in Fig. 1 takes a few minutes on a contemporary quad-core desktop workstation. All simulations for DOR and MAS experiments were performed using a single ^{14}N spin and neglecting the effects of protons and deuterons, using parameters summarised in Table 1. Hence the simulated DOR lineshapes are unaffected by the residual dipolar interactions with other neighbouring nuclei.

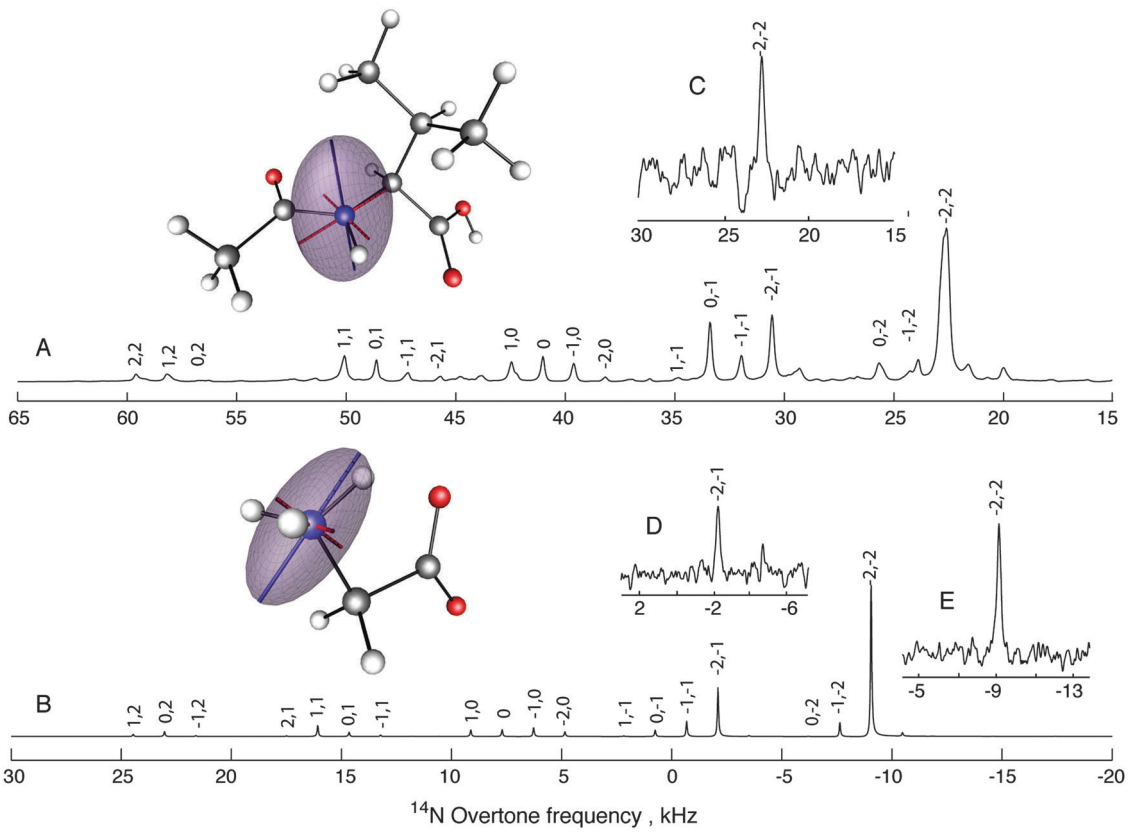

Fig. 1 DOR simulation and experiments for the ^{14}N overtone transition of glycine and NAV. Simulations were obtained using one ^{14}N spin, parameters from Table 1 and ideal pulses. Experiments were recorded at $\omega_{\mathrm{nut}}^{\mathrm{OT}}/2\pi$ = 21 kHz without decoupling. The numbers above the peaks are indices for spinning sidebands of the outer and inner rotors, respectively. (A) Simulation for NAV using the outer rotor frequency of 1.45 kHz and the inner rotor frequency of 7.6 kHz; (B) simulation for glycine using the outer rotor frequency of 1.425 kHz and the inner rotor frequency of 6.95 kHz; (C) the experimental spectra of the (−2, −2) spinning sideband of deuterated NAV acquired with 550 000 scans using 300 μs pulse width; and (D and E) experimental spectra of the (−2, −2) and (−2, −1) spinning sidebands of deuterated glycine respectively, acquired with 40 000 scans using 800 μs pulse width. The ellipsoid plots indicate the principal directions and the absolute values of the corresponding eigenvalues for the ^{14}N NQI tensors.

Table 1 Summary of parameters used for the simulations of glycine and NAV, using a single nitrogen spin. CSA interaction tensor orientations are quoted relative to the eigenframe of the ^{14}N quadrupolar interaction tensor. The inner and outer rotor speed values match the experimental data. Floquet theory convergence is achieved at rank 5 in the MAS simulations, and rank 5 was also used for the inner and the outer rotations in the DOR simulations

	C_q MHz	η_q	σ_{iso} ppm	$\Delta\sigma$ ppm	η	Euler angles, CSA	Lebedev Grid Rank	(ν_{out}, ν_{in}) kHz
Gly[45,46]	1.18	0.53	32.4	–	–	–	11	(1.425, 6.95)
NAV[47–50]	3.21	0.32	121.8	105	0.23	[−90, −90, −17]	65	(1.450, 7.60)

Results and discussion

DOR NMR spectra were simulated for *N*-acetylvaline (NAV) and glycine (Fig. 1) using spin Hamiltonian parameters given in Table 1. Under MAS, the spectrum consists of five sidebands, the strongest peak belonging to the +2 sideband for the counter-clockwise (it matters) spinner rotation direction.[17] Under DOR, each sideband is split into a further family of sidebands whose line width is reduced compared to those obtained under MAS.

Experimental spectra (Fig. 1, insets) of deuterated glycine-d_3 and NAV-d_{13} were acquired at 850 MHz on a Bruker Avance III spectrometer equipped with a DOR probe where both spinners rotate in a clockwise direction. Due to the limited excitation bandwidth, it is not possible to record the overall spectrum at once and only individual sidebands can be recorded. The overtone transition is forbidden in the Zeeman basis and overtone excitation is quite ineffective with the low power levels provided by the DOR probe, leading to the long pulse length and narrow bandwidth. Nutation curves for the (−2, −2) spinning sidebands of both compounds are given in Fig. S1 (ESI†). Glycine requires longer pulses than NAV due to a smaller quadrupole coupling constant. As seen in Fig. 1, experimental results and simulation show good agreement for both the resonance position and relative peak intensity. The most intense signal is at the (−2, −2) spinning sideband. Attempts were also made to acquire other DOR spinning sidebands for glycine (8000 scans) but there was no clear evidence of the signal (Fig. S2, ESI†). The extent of the line-narrowing effect of DOR on overtone NMR data may be appreciated from Fig. 2 and 3. Note that simulations are consistently much narrower than the experimental data. The larger experimental line width is attributed to spinning frequency instabilities and dipolar couplings to other nuclei. Spinning speed variations of the DOR rotors were of the order of ±25 Hz, and since we are observing not the center-band but sidebands of the overtone signal, unstable spinning will significantly broaden the resonances. Moreover, the DOR experiments were run at moderate spinning frequencies and without any decoupling, hence dipolar coupling to deuterium and protons is unlikely to be fully averaged out. Such an extended spin system is too complex for accurate numerical simulation. Simulations of DOR in Fig. 2 and 3 are sharp as they do not suffer from these effects, and assumed a single nitrogen atom, but the full quadrupolar Hamiltonian (not just first and second order terms) is considered here. The *Spinach* input file which generated Fig. 1 for glycine is included in the ESI† as an example.

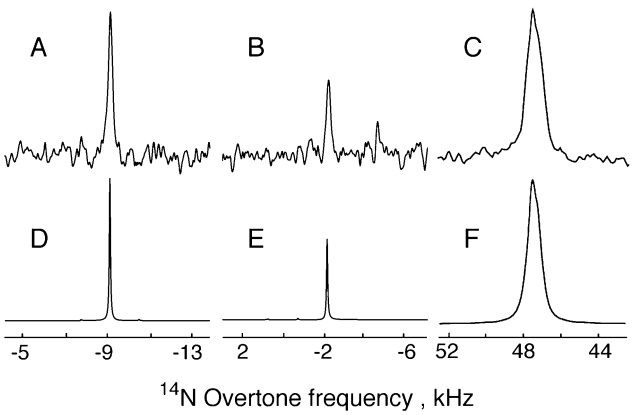

Fig. 2 Line width comparison for DOR and MAS overtone powder spectra of glycine. (A) DOR experiment for the (−2, −2) sideband of deuterated glycine, 40 000 scans, no decoupling; and (B) DOR experiment for the (−2, −1) sideband of deuterated glycine, 40 000 scans, no decoupling; DOR conditions are specified in the Fig. 1 caption. (C) MAS experiment for the +2 spinning sideband of glycine, 1024 scans, SPINAL64 decoupling, using $\omega_{nut}^{OT}/2\pi$ = 70 kHz and a 275 μs excitation pulse with $\omega_r/2\pi$ = 19.84 kHz. (D–F) Simulations of the data in A–C were performed using one ^{14}N spin, the parameters given in Table 1, and using durations and amplitudes matching the experimental data.

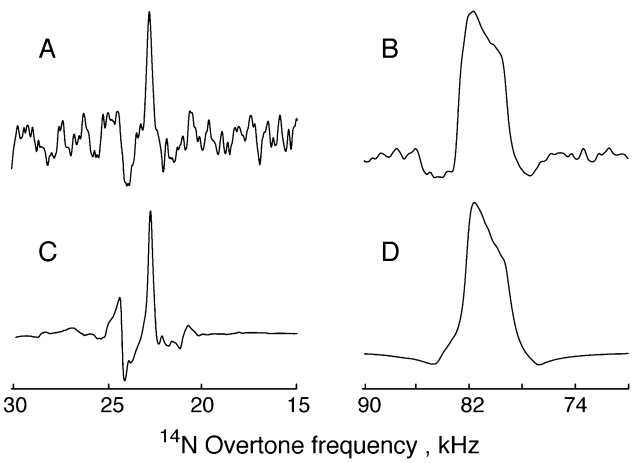

Fig. 3 Line width comparison for DOR and MAS overtone powder spectra of NAV. (A) DOR experiment data for the (−2, −2) spinning sideband of deuterated NAV, 550 000 scans, no decoupling. DOR conditions are specified in the Fig. 1 caption. (B) MAS experiment at the +2 spinning sideband of NAV, 40 000 scans, SPINAL64 decoupling, using $\omega_{nut}^{OT}/2\pi$ = 70 kHz and a 275 μs excitation pulse with $\omega_r/2\pi$ = 19.84 kHz; and (C) and (D) are the corresponding simulations, using one ^{14}N spin, the parameters given in Table 1, and using durations and amplitudes matching the experimental data. Note that the two features on the side of the main peak in (A) and (C) are spinning sidebands of the outer rotor.

For glycine, both the experimental and the simulated DOR NMR lines at (−2, −1) and (−2, −2) sidebands are about three times narrower than the corresponding MAS lines (Fig. 2). The experimental width of the (−2, −2) sideband under DOR is 280 Hz, while the width of the +2 spinning sideband under MAS is about 900 Hz (Fig. 2). It is clear from Fig. 3 that the (−2, −2) DOR sideband is much sharper than the +2 MAS sideband for NAV also: the 3.57 kHz line width under MAS is reduced to only 0.42 kHz under DOR, an improvement by almost an order of magnitude.

The reduction in line width observed under DOR indicates that the residual width apparent in the MAS ^{14}N overtone spectra does indeed arise from the second order quadrupolar terms in the Hamiltonian, removed in the DOR experiment. Importantly, none of that narrowing can be attributed to the narrow bandwidth of the very long overtone pulses under DOR, nor to the deuteration in the sample. This is because identical reduction in the line width is seen in the simulations in which the dipolar interactions with the surrounding atoms are switched off and ideal, very strong pulses are used (Fig. 1). The large number of scans required to record the DOR data arises from the reduced sample volume and reduced excitation efficiency compared to the MAS experiments, where stronger RF pulses are possible.[16]

Conclusions

These DOR results demonstrate the potential of ^{14}N double rotation overtone NMR in terms of resolution, with experimental line widths of a few hundred Hz achievable under DOR conditions. This represents a reduction by a factor of 3 and 9, as compared to MAS, for glycine and NAV, respectively, and a reduction in line width (determined by the third-order quadrupolar terms that survive double rotation averaging) to just tens of Hz predicted from theoretical simulations when artificial broadening is switched off, which sets the theoretical limit of what can be achieved under ideal conditions, without the intrinsic hardware limitation of DOR probes. The ongoing experimental developments go side by side with recent advances in theoretical and computational modelling. It is now possible to simulate elaborate overtone pulse sequences and soft pulses under MAS and double rotation in reasonable time.[37]

The routine application of DOR presents a number of technical challenges both in terms of sensitivity and RF performance. However pulsed methods for the suppression of 2nd order quadrupolar broadening effects in the indirect dimension (MQMAS and STMAS) have existed for half-integer spins for some time and can be implemented using standard solid-state NMR probes.[26–29] Our findings highlight that for integer spin nuclei, such as the ^{14}N case explored herein, similar averaging of the second order quadrupolar broadening is feasible and the development of pulsed methods will enable the routine realization of the significant resolution enhancements we have observed.

Acknowledgements

MC thanks the University Research Fellowship scheme from the Royal Society for support. LJB thanks the Royal Society for a Dorothy Hodgkin fellowship. Ibraheem Haies thanks The Higher Committee for Education Development in Iraq for financial support. The UK 850 MHz solid-state NMR Facility instruments used in this research were funded by EPSRC and BBSRC, as well as the University of Warwick, including *via* part funding through Birmingham Science City Advanced Materials Projects 1 and 2 supported by Advantage West Midlands (AWM) and the European Regional Development Fund (ERDF). The authors acknowledge the use of the IRIDIS High Performance Computing Facility, and associated support services at the University of Southampton, in the completion of this work. The development of *Spinach* is supported by EPSRC (EP/H003789/1).

References

1 L. A. O'Dell, *Prog. Nucl. Magn. Reson. Spectrosc.*, 2011, **59**, 295–318.
2 T. Giavani, H. Bildsøe, J. Skibsted and H. J. Jakobsen, *J. Magn. Reson.*, 2004, **166**, 262–272.
3 R. W. Schurko, *Acc. Chem. Res.*, 2013, **46**, 1985–1995.
4 S. Cavadini, *Prog. Nucl. Magn. Reson. Spectrosc.*, 2010, **56**, 46–77.
5 L. A. O'Dell and C. I. Ratcliffe, *Chem. Commun.*, 2010, **46**, 6774–6776.
6 S. Cavadini, A. Abraham and G. Bodenhausen, *Chem. Phys. Lett.*, 2007, **445**, 1–5.
7 S. Cavadini, A. Abraham and G. Bodenhausen, *J. Magn. Reson.*, 2008, **190**, 160–164.
8 S. Cavadini, S. Antonijevic, A. Lupulescu and G. Bodenhausen, *J. Magn. Reson.*, 2006, **182**, 168–172.
9 S. Cavadini, S. Antonijevic, A. Lupulescu and G. Bodenhausen, *ChemPhysChem*, 2007, **8**, 1363–1374.
10 S. Cavadini, A. Lupulescu, S. Antonijevic and G. Bodenhausen, *J. Am. Chem. Soc.*, 2006, **128**, 7706–7707.
11 S. Cavadini, V. Vitzthum, S. Ulzega, A. Abraham and G. Bodenhausen, *J. Magn. Reson.*, 2010, **202**, 57–63.
12 Z. Gan, *J. Am. Chem. Soc.*, 2006, **128**, 6040–6041.
13 Z. Gan, J. P. Amoureux and J. Trébosc, *Chem. Phys. Lett.*, 2007, **435**, 163–169.
14 J. A. Jarvis, I. M. Haies, P. T. Williamson and M. Carravetta, *Phys. Chem. Chem. Phys.*, 2013, **15**, 7613–7620.
15 D.-K. Lee and A. Ramamoorthy, *Chem. Phys. Lett.*, 1998, **286**, 398–402.
16 Y. Nishiyama, M. Malon, Z. Gan, Y. Endo and T. Nemoto, *J. Magn. Reson.*, 2013, **230**, 160–164.
17 L. A. O'Dell and A. Brinkmann, *J. Chem. Phys.*, 2013, **138**, 064201.
18 L. A. O'Dell, R. L. He and J. Pandohee, *CrystEngComm*, 2013, **15**, 8657–8667.
19 L. A. O'Dell and C. I. Ratcliffe, *Chem. Phys. Lett.*, 2011, **514**, 168–173.

20 A. J. Rossini, L. Emsley and L. A. O'Dell, *Phys. Chem. Chem. Phys.*, 2014, **16**, 12890–12899.
21 R. Tycko and S. J. Opella, *J. Am. Chem. Soc.*, 1986, **108**, 3531–3532.
22 R. Tycko and S. J. Opella, *J. Chem. Phys.*, 1987, **86**, 1761.
23 R. Tycko, P. L. Stewart and S. J. Opella, *J. Am. Chem. Soc.*, 1986, **108**, 5419–5425.
24 I. Haies, J. Jarvis, H. Bentley, I. Heinmaa, I. Kuprov, P. T. F. Williamson and M. Carravetta, *Phys. Chem. Chem. Phys.*, 2015, **7**, 6577–6587.
25 M. Bloom and M. A. LeGros, *Can. J. Phys.*, 1986, **64**, 1522–1528.
26 L. Frydman and J. S. Harwood, *J. Am. Chem. Soc.*, 1995, **117**, 5367–5368.
27 A. Medek, J. S. Harwood and L. Frydman, *J. Am. Chem. Soc.*, 1995, **117**, 12779–12787.
28 G. Wu, D. Rovnyank, B. Q. Sun and R. G. Griffin, *Chem. Phys. Lett.*, 1996, **249**, 210–217.
29 Z. H. Gan, *J. Am. Chem. Soc.*, 2000, **122**, 3242–3243.
30 A. Samoson, E. Lippmaa and A. Pines, *Mol. Phys.*, 1988, **65**, 1013–1018.
31 B. F. Chmelka, K. T. Mueller, A. Pines, J. Stebbins, Y. Wu and J. W. Zwanziger, *Nature*, 1989, **339**, 42–43.
32 A. Samoson and A. Pines, *Rev. Sci. Instrum.*, 1989, **60**, 3239–3241.
33 K. T. Mueller, B. Q. Sun, G. C. Chingas, J. W. Zwanziger, T. Terao and A. Pines, *J. Magn. Reson.*, 1990, **86**, 470–487.
34 P. de Fouquieres, S. G. Schirmer, S. J. Glaser and I. Kuprov, *J. Magn. Reson.*, 2011, **212**, 412–417.
35 L. J. Edwards, D. V. Savostyanov, A. A. Nevzorov, M. Concistre, G. Pileio and I. Kuprov, *J. Magn. Reson.*, 2013, **235**, 121–129.
36 A. A. Nevzorov, *J. Magn. Reson.*, 2014, 249.
37 H. J. Hogben, M. Krzystyniak, G. T. Charnock, P. J. Hore and I. Kuprov, *J. Magn. Reson.*, 2011, **208**, 179–194.
38 P. Bertani, J. Raya and B. Bechinger, *Solid State Nucl. Magn. Reson.*, 2014, **61–62**, 15–18.
39 M. Erdelyi, V. Langer, A. Karlen and A. Gogoll, *New J. Chem.*, 2002, **26**, 834–843.
40 G. Moro and J. H. Freed, *J. Chem. Phys.*, 1981, **74**, 3757–3773.
41 C. F. Polnaszek, G. V. Bruno and J. H. Freed, *J. Chem. Phys.*, 1973, **58**, 3185–3199.
42 M. Leskes, P. K. Madhu and S. Vega, *Prog. Nucl. Magn. Reson. Spectrosc.*, 2010, **57**, 345–380.
43 I. Scholz, J. D. van Beek and M. Ernst, *Solid State Nucl. Magn. Reson.*, 2010, **37**, 39–59.
44 L. N. Trefethen, *Spectral methods in MATLAB*, Siam, 2000.
45 R. A. Haberkorn, R. E. Stark, H. Vanwilligen and R. G. Griffin, *J. Am. Chem. Soc.*, 1981, **103**, 2534–2539.
46 R. E. Taylor and C. Dybowski, *J. Mol. Struct.*, 2008, **889**, 376–382.
47 R. E. Stark, R. A. Haberkorn and R. G. Griffin, *J. Chem. Phys.*, 1978, **68**, 1996.
48 E. Salnikov, P. Bertani, J. Raap and B. Bechinger, *J. Biomol. NMR*, 2009, **45**, 373–387.
49 M. Bak, R. Schultz, T. Vosegaard and N. C. Nielsen, *J. Magn. Reson.*, 2002, **154**, 28–45.
50 G. Hou, I. J. Byeon, J. Ahn, A. M. Gronenborn and T. Polenova, *J. Chem. Phys.*, 2012, **137**, 134201.